

**Texas A&M University
Mechanical Engineering Department
Turbomachinery Laboratory
Tribology Group**

**COMPARISON OF LEAKAGE BETWEEN A
LABYRINTH SEAL AND AN ALL-METAL
COMPLIANT GAS SEAL AT HIGH
TEMPERATURE**

Research Progress Report to the TAMU Turbomachinery Research Consortium

02
TRC- Seal-XX-11

By

Luis San Andrés

Mast-Childs Tribology Professor
Principal Investigator

Alain Anderson

Research Assistant

May 2011

MEASUREMENTS OF LEAKAGE IN A NOVEL ALL METAL NON CONTACTING ANNULAR SEAL AT HIGH
TEMPERATURES

TRC Project, TEES # 32513/1519 3S

EXECUTIVE SUMMARY

COMPARISON OF LEAKAGE BETWEEN A LABYRINTH SEAL AND AN ALL-METAL COMPLIANT GAS SEAL AT HIGH TEMPERATURE

LUIS SAN ANDRES, MAY 2011

Parasitic secondary flow losses (seal leakage) reduce efficiency and power delivery in turbomachinery. Labyrinth seals (LBS) are the most common and inexpensive seal type, albeit wearing out with operation thus penalizing performance and even affecting rotordynamic stability. Costlier brush seals (BS), common in gas and steam turbines, can reduce secondary flow leakage by 50% or more than with a similar size LB. Novel non-contact all metal compliant seals, such as the Hybrid Brush Seal (HBS), offer further reductions in leakage, and due to the hydrodynamic lift of components, show no wear and no local thermal distortion. Prior funded research at TAMU (2007-09) quantified the leakage of three types of seals, similar in size, operating at a high temperature (300°C): a three-tooth labyrinth seal leaked worst, ~twice as much as a BS and ~ three times more than a HBS.

In July 2010, TRC funded a two-year program to (a) conduct non-proprietary leakage tests with a HALO™ seal and, for comparison, a three tooth labyrinth seal; and (b) to revamp an existing test rig for operation at rotor speeds reaching a tip surface speed of 120 m/s, as is typical in land-based power generation gas and steam turbines. The HALO™ seal is a novel seal type, originating from the HBS, as a softly supported, multiple-pad all-metal seal with both hydrostatic and hydrodynamic lift characteristics to generate a self-controlling clearance seal.

In 2011, with a non rotating shaft, seal flow rate measurements with increasing inlet air temperatures (to 300°C) show the HALO™ seal leaks 50% or less than the labyrinth seal. For pressure ratios (P_s/P_a) > 3.0, the HALO™ seal leaks ~1/4 the flow in a labyrinth seal, thus demonstrating its excellent sealing characteristics. Moreover, tests with the novel seal proceeded to higher pressure ratios (max. $P_s/P_a=8$), a feature that could not be achieved with the LBS.

The leakage measurements demonstrate the HALO™ gives a remarkable improvement to seal secondary flows and the ability to operate at high pressure ratios. Further research, analytical and experimental, will be performed in the second year further advance the novel seal technology.

TABLE OF CONTENTS

COMPARISON OF LEAKAGE BETWEEN A LABYRINTH SEAL AND AN ALL-METAL COMPLIANT GAS SEAL AT HIGH TEMPERATURE

LUIS SAN ANDRES, MAY 2011

	<u>page</u>
EXECUTIVE SUMMARY	ii
LIST OF TABLES	iv
LIST OF FIGURES	iv
JUSTIFICATION AND STATEMENT OF WORK	1
BUDGET, SCHEDULE AND COMPLETION OF TASKS	2
DESCRIPTION OF HIGH TEMPERATURE GAS SEAL TEST RIG	3
DESCRIPTION OF TESTS SEALS	6
LEAKAGE MEASUREMENTS WITH LABYRINTH SEAL AND HALO™ SEAL	10
REVAMPING TEST RIG FOR MEASUREMENTS AT HIGH ROTOR SPEEDS	13
CLOSURE	18
REFERENCES	19
APPENDIX A. A BRIEF REVIEW OF LITERATURE ON NON-CONTACTING GAS SEALS: LABYRINTH, BRUSH AND AN ALL METAL SEAL	20
APPENDIX B. CALIBRATION CHARTS FOR INSTRUMENTATION	27

LIST OF TABLES

No		page
1	Budget for TRC project (2010)	2
2	Schedule of work and completed tasks	2
3	Dimensions and material properties of labyrinth seal and disc	7
4	Halo seal geometry and material properties	8
5	Air conditions for seal leakage measurements	10
6	Dimensions and material specifications for test MMFB	15
7	Predicted critical speed and damping ratio for rotor supported on MMFB. Shaft diameter varies. Predicted rotor mode shapes at 10 krpm	17

LIST OF FIGURES

No		page
1	Cutaway views of high temperature seal test rig and photograph of disc and centering rods	4
2	Rotor structural model and depiction of gas flow path in high temperature seal test rig	5
3	Photographs of three-tooth labyrinth seal: views from upstream and inner side. Right inset shows the teeth and cavities along the axial direction	7
4	Photographs of HALO™ seal: views from upstream, downstream and inner side	9
5	Axial profile of a resilient pad in HALO™ seal (Courtesy of ATG)	9
6	Measured radial clearance in HALO™ seal versus pressure ratio $[P_s/P_e]$. Ambient temperature (30 °C) and without disc rotation. Data from Ref. [2]	10
7	Labyrinth seal: mass flow rate vs. pressure ratio (P_s/P_a) . Tests at increasing air temperatures. Comparison to prior data in Ref. [4]. Discharge at ambient pressure (P_a) .	11
8	HALO™ seal: mass flow rate vs. pressure ratio (P_s/P_a) . Tests at increasing air temperatures. Discharge at ambient pressure (P_a) .	11
9	Labyrinth seal: Flow factor Φ_M vs. pressure ratio (P_s/P_a) . Tests at increasing air temperatures. Comparison to prior data in Ref. [4]	13
10	HALO™ seal: Flow factor Φ_M vs. pressure ratio (P_s/P_a) . Tests at increasing air temperatures	13
11	Rotor model with metal mesh foil bearing at free end of rotor	15
12	Photograph of Metal Mesh Foil Bearing	15
13	Various rotor models (shaft OD increases) considered for analysis	16
14	Amplitude of rotor synchronous response at disc location for various shaft OD	18

configurations. Imbalance $u=0.01$ gm-cm at disc outboard

A.1	Inner side view of a three tooth labyrinth seal and schematic view of thru flow	21
A.2	Inner side view of a brush seal and schematic view of thru flow	22
A.3	Inner side view of a hybrid brush seal and schematic view of thru flow	24
A.4	Inner side view of a HALO TM seal and schematic view of thru flow	25
B.1	Voltage (V) versus static pressure for pressure sensor to record supply pressure in high temperature gas seal test rig	27
B.2	Voltage (mV) versus static pressure for pressure sensors to record pressure in flow meter and exhaust chamber	28
B.3	Volumetric flow rate (SCFM) versus frequency (Hz) in turbine flowmeter	29

JUSTIFICATION AND STATEMENT OF WORK

Parasitic secondary flows (seals leakage) in centrifugal compressors and gas and steam turbines represent a substantial loss in efficiency and power delivery with an increase in specific fuel consumption. Labyrinth seals (LBS) are the most common and inexpensive means of reducing secondary leakage, albeit wearing out with operation and thereby penalizing performance and even affecting rotordynamic stability. Brush seals (BS), although costlier, are common in specialized applications (aircraft engines). BS may increase plant efficiency by up to 1/6 of a point and with as little as 1/3 of the leakage in a similar size labyrinth seal. [1]

Presently, other non-contacting seal types; all metal and compliant, such as finger-seals and the HALO™ [Hydrostatic Advanced Low Leakage] seal [2], have been engineered to reduce even more the leakage in steam and gas turbines, in particular for operation with high pressure ratios and high tip surface rotor speeds.

Siemens Power Generation, Inc. and Advanced Technologies Group (ATG) sponsored research (2007-2009) to build a high temperature seal test rig (max 300°C) spinning at low rotational speeds (max 26 m/s tip speed), see Figure 1 later. The research quantified the leakage of various seal technologies, comparing results among the tested seals, and recommending the most reliable sealing technology for ready implementation in power generation gas turbine [3].

In 2010, the Turbomachinery Research Consortium funded a proposal to continue researching novel non-contacting metal seals in a two-year project with the following objectives:

- a) To revamp the existing test rig for operation at high rotor speeds reaching a tip surface speed of 120 m/s (15 krpm).
- b) To perform clearance and leakage measurements with a three teeth labyrinth seal and the HALO™ seal operating with inlet pressure to 5 bar and temperature to 300°C.
- c) To compare the leakage performance of both seals and to validate XLLABY® leakage predictions with the high temperature results.

The research product –a reliable leakage data base- will enable the application of state of the art sealing technology that increases system efficiency by reducing leakage and that extends maintenance intervals by eliminating wear of components.

BUDGET, SCHEDULE AND COMPLETION OF TASKS

Table 1 details the approved budget for the project with 81% dedicated to the support of a graduate student and 16% allocated for facilities revamping. The project started on September 1, 2010 with the enrollment of Mr. Alain Anderson, M.S. graduate student, as the Research Assistant funded by the project. An undergraduate student worker, Mr. James Law, also assisted the graduate student in operating the test facility and making some modifications.

Table 1. Budget for TRC project (2010)

Support for graduate student (20 h/week) x \$ 1,700 x 12 months	\$ 20,400
Fringe benefits (0.6%) and medical insurance (\$191/month)	\$ 2,412
Travel to (US) technical conference	\$ 1,500
Tuition three semesters (\$3,488 x 3)	\$ 9,301
Equipment: test rig revamping to high speed – estimate only	<u>\$ 6,250</u>
Total Cost:	\$ 39,863

Table 2 shows the schedule of work and activities completed by the graduate student to date. The student read the literature relevant to gas seals and their applications, learned to assemble and operate the test rig, completed several leakage measurements, and is presently working on the redesign of the test rig for high speed operation.

Table 2. Schedule of work and completed tasks

C: completed, P: progress, NC: not completed

Item	2010		2011			2012		Total
	Sept-Nov	Dec-Feb	Mar-May	June-Aug	Sept-Nov	Dec-Feb	Mar-May	
Archival literature: read and review			P →					
Review test rig operation and assembly		C →						
Review DAQ system operation and troubleshooting		C →						
Assemble test rig: labyrinth seal - measure leakage for increasing temperatures (300 C)			P →					
Assemble test rig: HALO Seal - measure leakage for increasing temperatures (300 C)			P →					
Re-design of test rig for high speed operation			P →					
Learn XLTRC2 and predict rotordynamic response of modified rotor for 125m/s tip speed			P →					
Design review for safety				→				
Construct modified rig and troubleshoot for high speed operation				→				
Tests to 15 krpm - Labyrinth seal (max 300 C)				→				
Tests to 15 krpm - HALO seal (max 300 C)				→				
Predictions for Labyrinth seal			NC	→				
Documentation		proposal	TRC report	ASME paper			Thesis-TRC	
		To do	P	To do			To do	
	# hours in 3 month period							
24 months	Sept-Nov	Dec-Feb	Mar-May	June-Aug	Sept-Nov	Dec-Feb	Mar-May	# hours
12 months x 50% effort = 20 h/week	278	278	278	278	278	278	278	1946

Appendix A contains a recent literature review on gas seals written by the student.

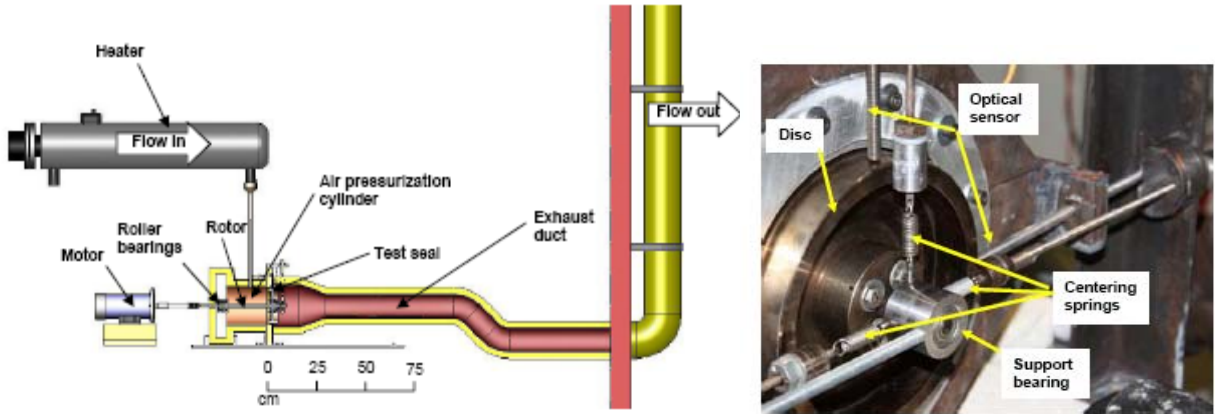
DESCRIPTION OF HIGH TEMPERATURE GAS SEAL TEST RIG

Figure 1 shows a cut view of the high temperature seal test rig. Two tapered rolling element bearings support an overhung shaft and disc inside a pressurization vessel supplied with hot air. A quill shaft and flexible coupling connect the test rotor to a drive DC motor (90V, 9.4A).

Figure 2 depicts the structural rotor model and displays the flow path into and out of the test rig. A test seal fits in a circumferential groove machined at the end of the pressurized vessel and is held in place by a thin plate and fastening bolts. A seal faces directly the end disc outer diameter $OD = 166.8$ mm. The cantilever shaft-disc arrangement allows the rapid exchange of test seals without disturbing the major components of the system.

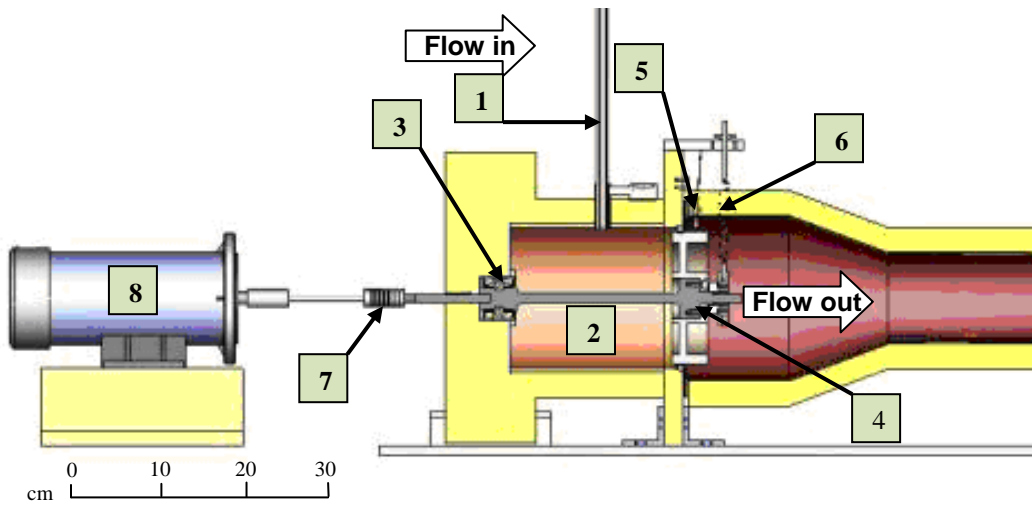
Just outside of the disc-rotor, in the exhaust duct, an (unlubricated) 8 mm ID ball bearing and rods assembly loosely guides the free end of the shaft-disc assembly. This bushing is supported by horizontal and vertical threaded steel rods attached to an external frame. Turning the rods at the frame location displaces the bushing thus permitting centering of the disc with respect to the seal.

The support bearings are rolling element tapered bearings, see inset, tolerating high temperatures when packed with a special (expensive) grease [Krytox 240-AC]. The bearings' outer races fit into a cylindrical casing in the pressure vessel while the inner races are press fitted onto the shaft end. The bearings are installed with their tapered rolling elements in opposite directions to support the large axial thrust loads induced by the air pressure on the inner side of the large disc; for example, at a 100 psig supply pressure, the axial load is 510 lb_f . In addition, an aluminum silicate plate on the closed end of the pressure vessel acts as an insulation element prevents excessive heating of the bearings.



(a) Complete view of test rig

(b) View of rotor disc and centering rods



1	Hot air inlet	5	Optical displacement sensor
2	Pressurization cylinder and shaft	6	Centering mechanism
3	Radial Support bearings	7	Flexible coupling
4	Disc and test seal location	8	Electric drive motor

Figure 1. Cutaway views of high temperature seal test rig and photograph of disc and centering rods [1]

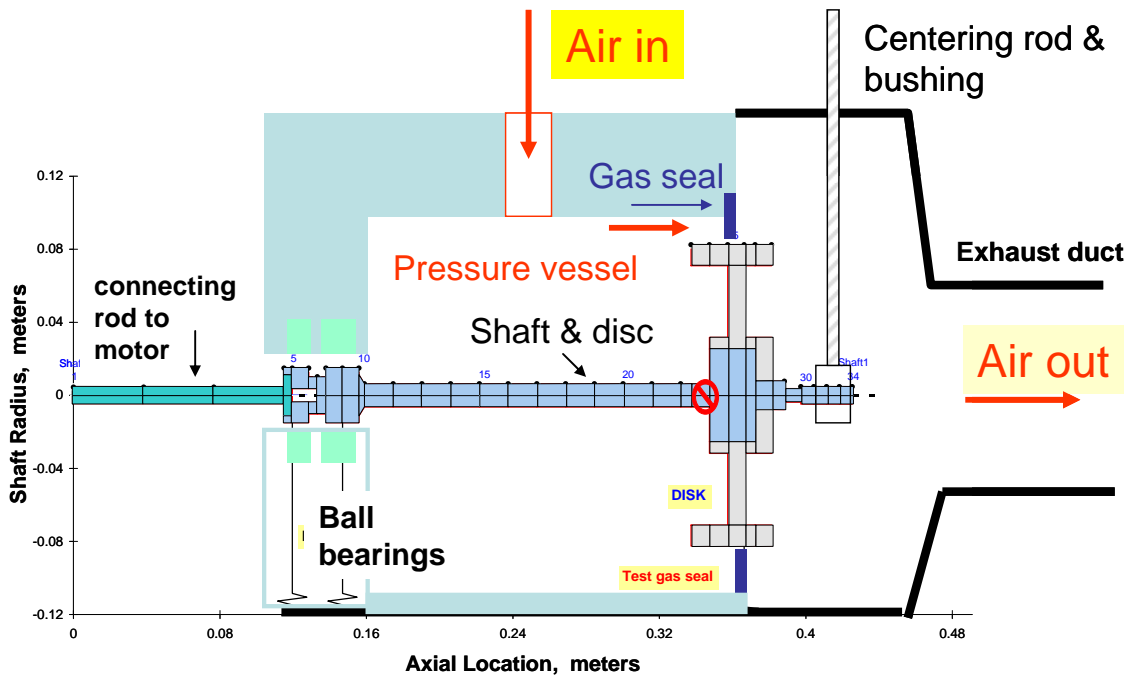
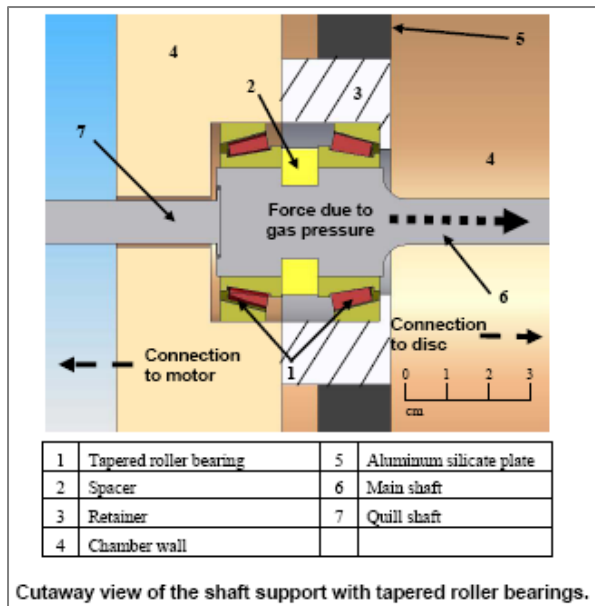


Figure 2. Rotor structural model and depiction of gas flow path in high temperature seal test rig



Two fiber optic sensors, orthogonally positioned, measure the radial displacements of the disc. An electric heater (12 kW, 240 V) warms air to a set temperature (max 300 °C) with delivery at a maximum pressure of 7.6 bar. A thick layer of thermal insulation fully covers the test rig and the insulated exhaust duct routes the hot discharged air at ambient pressure, through a tall chimney, for disposal outside the laboratory.

In the experimental procedure, the air inlet temperature and pressure upstream of a test seal, the rotor speed, and the disc centering are independently controlled.

Operation of the test rig begins once a seal is installed facing the OD of the large disc. A careful centering of the disc with respect to the seal ensures a uniform radial gap. Pressurized cold air flows through a particle and coalescing filter to remove impurities such as water and oil.

Next, the air stream passes through a turbine flow meter recording its volumetric flow rate. The mass flow rate is found from the volumetric flow rate for a specific pressure and temperature at standard air conditions.

The cold air then flows through an electromechanical control valve and to an electric heater (12 kW, 240 V). The valve opens at 14 distinct positions until fully open to control the air flow and upstream pressure. The electrical heater warms the air to a set temperature, max. 300 °C. The hot air then enters the pressurization cylinder where the air inlet temperature and pressure are recorded. Finally, the hot air flows through the test seal and into the atmosphere through the exhaust pipe and chimney.

A PC Field Programmable Gate Array (FPGA) sets up and controls the electromechanical opening valve, the electrical heater, and the data acquisition. The operator sets the desired temperature and pressure in the vessel upstream of the seal with a dedicated NI Labview® Virtual Instrument (VI) [4]. The VI records and saves the collected data (pressures, temperatures and flow) for post-processing and display.

Refs. [3], [4] detail the experimental results from prior work with one labyrinth seal, one conventional brush seal and one hybrid brush seal (HBS). The aluminum labyrinth seal has three sharp teeth with a cavity depth of 3.0 mm and tip width of 0.17 mm. The brush seal and hybrid brush seal had similar material properties, bristles of Haynes-25, diameter 0.051 mm, 45° lay angle and density of 850 bristles/cm. Upon installation at ambient conditions, the seals had a diametral clearance equaling 1.04 mm for the labyrinth seal and 0.52 mm for the brush seals. Note that the operating clearance changes rapidly with temperature due to thermal growth of the components, see Ref. [4] for details.

In 2011, for the TRC funded project, two seals were tested in the existing test rig facility; one is a labyrinth seal and the other a HALO™ seal. Tests with the labyrinth seal are important to benchmark the leakage performance of the more advanced HALO™ seal.

DESCRIPTION OF TEST SEALS

Figure 3 shows a photograph of the three tooth labyrinth seal and Table 3 details the seal and disc dimensions and materials. Note that the disc and seal are made of steel and aluminum, respectively; hence their thermal expansion coefficients are dissimilar.

Table 3. Dimensions and material properties of labyrinth seal and disc (room temperature 25°C) [4]

Seal Material	Aluminum
Thermal expansion, α	$23.6 \cdot 10^{-6} / ^\circ\text{C}$
Outer diameter	183.20 mm
Inner diameter	167.85 mm
Length axial, l	8.40 mm
Tip width	0.17 mm
Cavity depth	3 mm
Disc Material	4140 Steel
Disc Thermal expansion, α	$12 \cdot 10^{-6} / ^\circ\text{C}$
Disc OD	166.81 mm
Diametrical clearance, $2c$	1.04 ± 0.026 mm

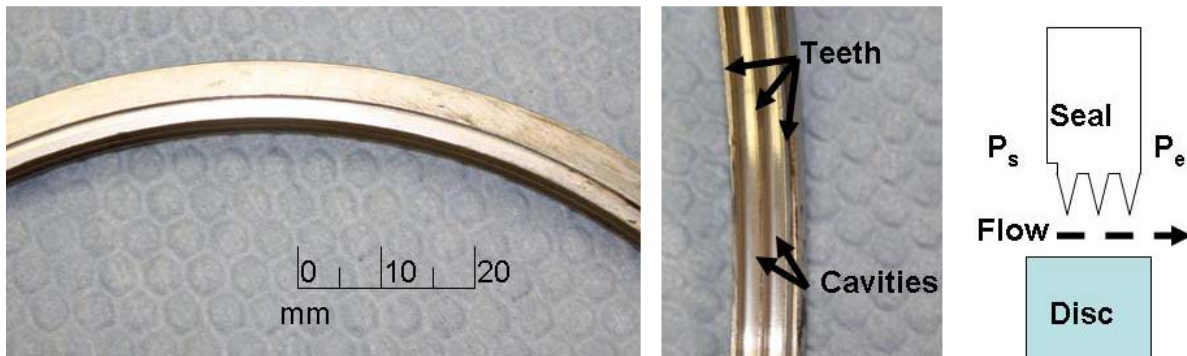


Figure 3. Photographs of three-tooth labyrinth seal: views from upstream and inner side. Right inset shows the teeth and cavities along the axial direction [3]

The Hydrostatic Advanced Low Leakage [HALO™] seal donated by ATG is a sealing technology replacing their hybrid brush seal (HBS). Figure 4 depicts close up photographs of the HALO™ seal and Table 4 lists its geometry and material properties. The HALO™ seal is an all-metal component manufactured with wire EDM procedure. The seal comprises of nine arcuate pads cantilevered from an outer rim. The compliance of the thin beams (flexures) allows for easy radial displacement of the pads. A downstream plate blocks any flow through the gaps behind the pads. As shown in Figure 5, the pads are not flat but have a machined converging-divergent profile that promotes the development of hydrodynamic pressure to lift-off the pads with rotor speed thus ensuring non-contact operation with the disc.

Table 4. HALO™ seal geometry and material properties [2]

Seal Material	Steel
Coefficient of thermal expansion	$12 \times 10^{-6} / ^\circ\text{C}$
Outer diameter	183.0 mm ± 0.013
Inner diameter (upstream)	167.3 mm ± 0.013
Inner diameter (downstream)	167.2 mm ± 0.013
Seal axial length, l	8.5 mm ± 0.013
Pad allowable radial movement	0.25 mm ± 0.013
Pad axial length	8.0 mm ± 0.013
Pad arc length	57.4 mm ± 0.013
Number of pads	9 pads ($\sim 40^\circ$)
Single pad stiffness (*)	53 N/mm ± 9
Beam axial width	6.5 mm ± 0.013
Ambient Clearance (T=25°C)	
OD – ID _s = seal diametral clearance	0.40 mm ± 0.025

(*) Pad stiffness found by measuring the EDM gap with a pair of feeler gages both before and after applying a small weight onto the pad.

Once installed in the test rig, the seal assembled radial clearance equals 0.20 mm (~ 8 mil). Note that the seal pads can displace a maximum of 0.25 mm (gap behind spring elements). The HALO™ is a clearance controlled seal; with external pressurization the flexures displace the pads towards the disc thus closing the gap, as shown by prior measurements, see Figure 6. Note that the seal engineered design aims to operate the HALO™ seal (always) near choked condition by producing a sufficiently small gap (clearance). This feature does not work well for too low pressure drops (say less than 10 psig [0.7 bar]).

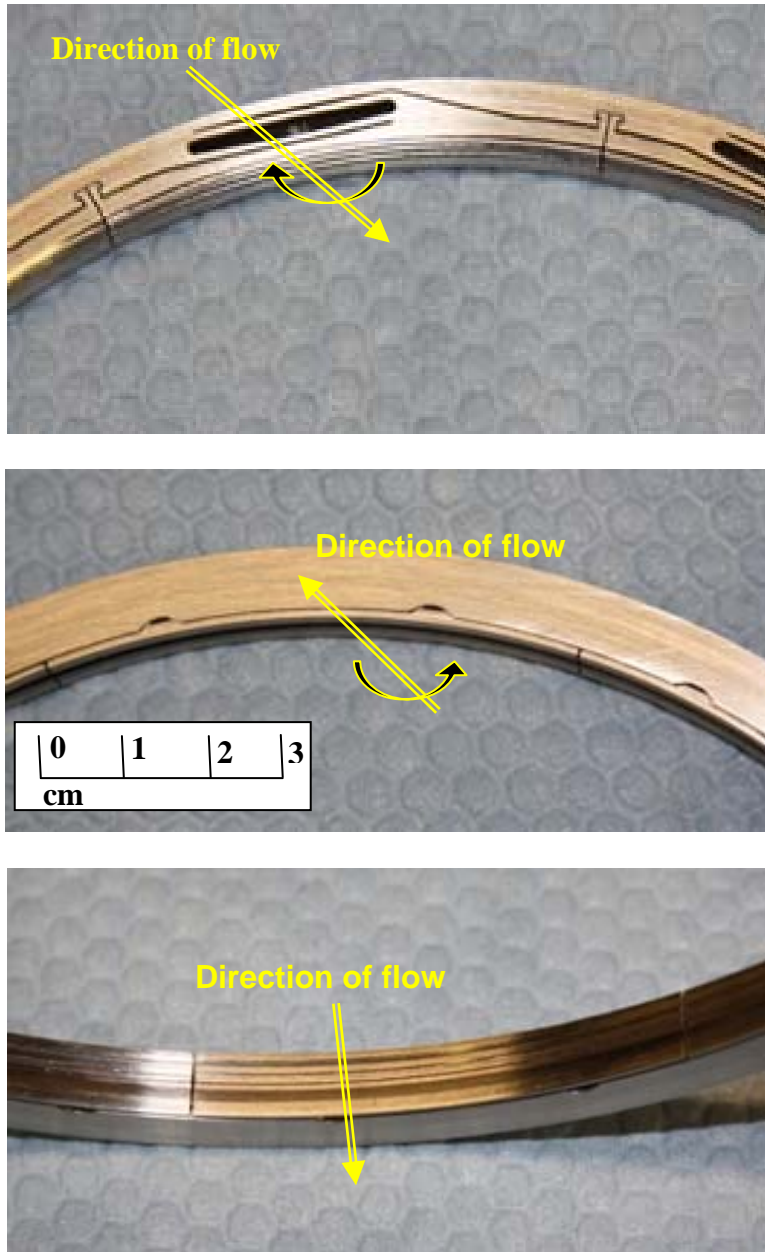
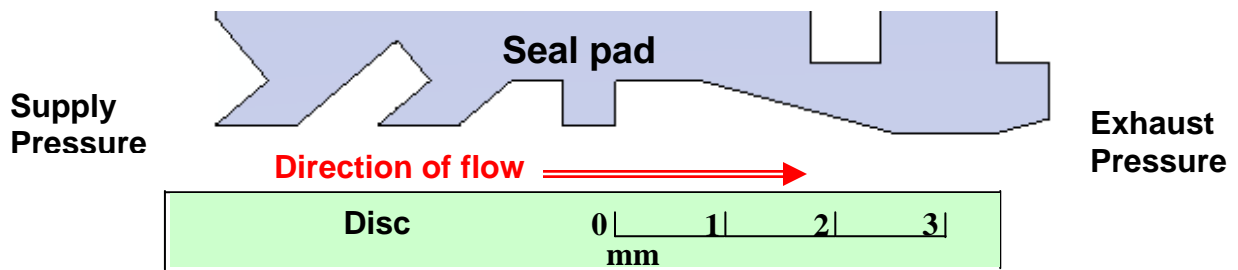


Figure 4. Photographs of HALO™ seal: views from upstream, downstream and inner side



*Clearance between seal pad and disc not to scale.

Figure 5. Axial profile of a resilient pad in HALO™ seal (Courtesy of ATG) [2]

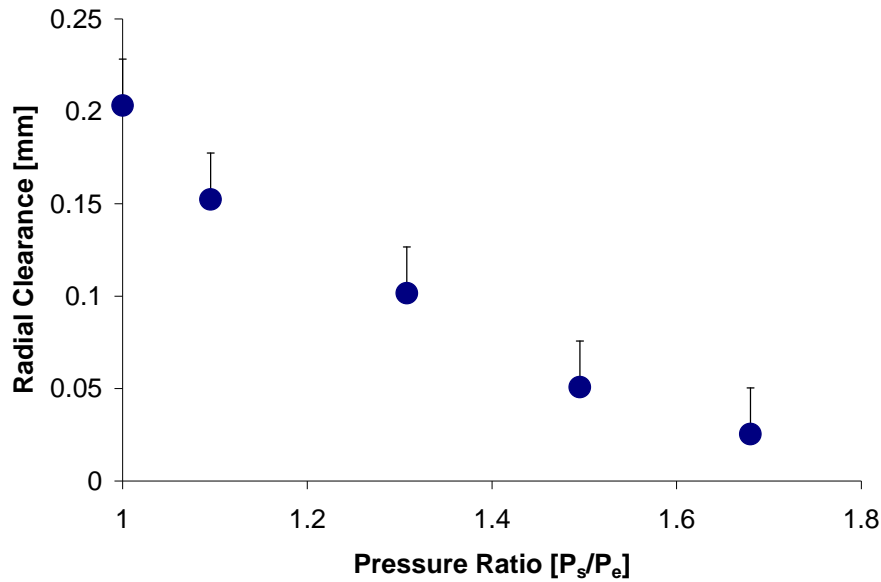


Figure 6. Measured radial clearance in HALO™ seal versus pressure ratio [P_s/P_e]. Ambient temperature (30 °C) and without disc rotation. Data from Ref. [2]

LEAKAGE MEASUREMENTS WITH LABYRINTH SEAL AND HALO™ SEAL

Table 5 lists the air supply conditions for leakage measurements in the three tooth labyrinth seal and the HALO™ seal. In the tests, the rotor was stationary (no spinning)¹. Measurements of seal leakage were conducted at increasing air inlet temperatures to a maximum of 300°C.

Table 5. Air conditions for seal leakage measurements

Specific gas constant, R_g	287 J/kg-°K	
Supply pressure, P_s	14.7-118 psi	101-813 kPa
Inlet temperature, T	77°-572°F	298°-573°K
Exhaust pressure, P_a	14.7 psi	101 kPa
Ambient temperature	77°F	298°K

Figures 7 and 8 depict the recorded seals' leakage (gram/s) versus the inlet to exhaust pressure ratio (P_s/P_a) for increasing air inlet temperatures (30°, 100°, 200° and 300°C). For comparison, Figure 7 includes prior test data reported in Ref. [4].

¹ Safety considerations prevented the operation of the drive motor. The rig needs to have an adequate guard covering the connecting coupling to contain any possible fracture of the transmission element. The Research Assistant faced many difficulties in learning the assembly and operation of the test rig. His lack of practical experience in handling mechanical components and limited knowledge on the way *things* work were major obstacles to produce useful results.

For all pressures ratios, the HALO™ seal leaks 50% or less than the labyrinth seal. For $(P_s/P_a) > 3.0$, the HALO™ seal leaks $\sim 1/4$ the flow rate of the labyrinth seal thus demonstrating its excellent sealing characteristics. Moreover, tests with the novel seal proceeded to higher pressure ratios (max. $P_s/P_a=8$), a feature that could not be achieved with the labyrinth seal.

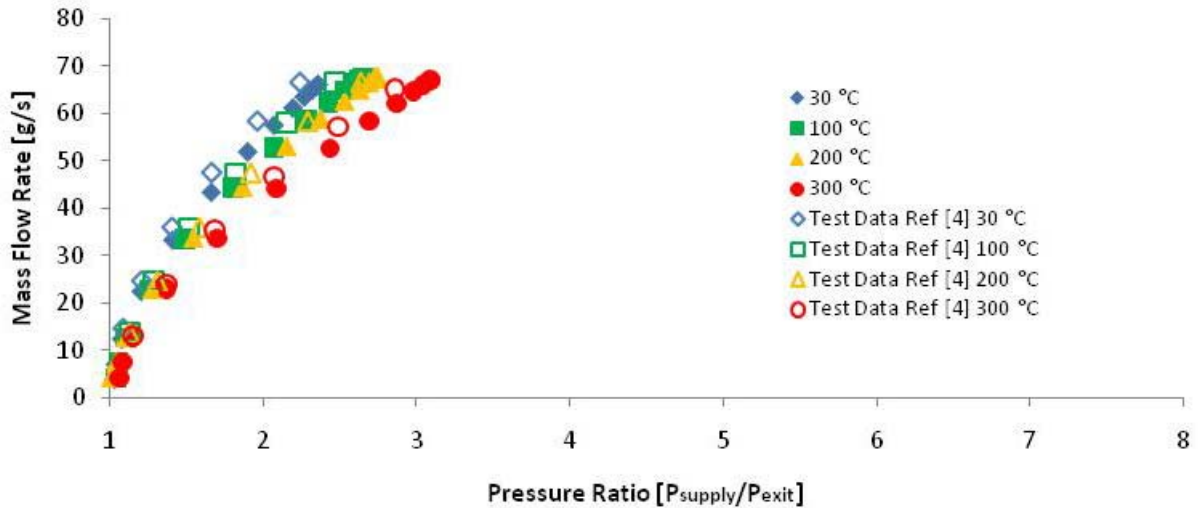


Figure 7. Labyrinth seal: mass flow rate vs. pressure ratio (P_s/P_a). Tests at increasing air temperatures. Comparison to prior data in Ref. [4]. Discharge at ambient pressure (P_a).

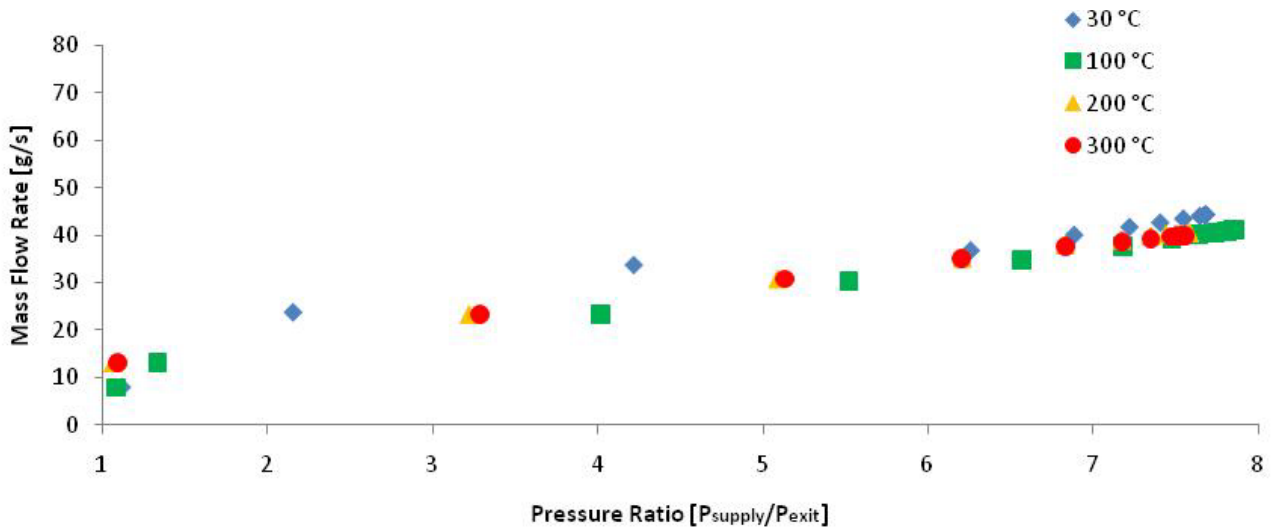


Figure 8. HALO™ seal: mass flow rate vs. pressure ratio (P_s/P_a). Tests at increasing air temperatures. Discharge at ambient pressure (P_a).

Uncertainties for the current test results portrayed above are yet to be determined. However, prior measurements with the same seals showed the following uncertainties, Refs. [2-4].

	Labyrinth Seal [3]		HALO™ Seal [2]	
	Maximum %	Average %	Maximum %	Average %
Pressure ratio	4.4	0.5	4.0	1.3
Mass flow rate	4.5	0.4	1.0	0.4

On average the maximum uncertainty for flow measurements is less than 5% for a 95% confidence interval.

Delgado and Proctor [5] recommend a flow factor Φ to compare the leakage performance of different types of seals, contacting or not, of unequal diameter and operating at dissimilar temperatures. The flow factor accounts for the gas supply pressure P_s [Pa] and inlet temperature T [°K], and the seal size (rotor diameter D). A modified flow Φ_M factor also accounts for dissimilar axial lengths, l , both in [m]). The modified flow factor is

$$\Phi_M = \frac{\dot{m}\sqrt{T}}{P_s D} l \quad (1)$$

where \dot{m} is the seal mass flow rate or leakage [kg/s], Note that the flow factor is dimensional, its physical units equal $\text{kg}\cdot\text{K}^{0.5}/(\text{MPa}\cdot\text{s})$. For the labyrinth seal, $l=8.4$ mm equals the seal physical length (teeth and cavities). For the HALO™ seal, the pad axial length is taken as a characteristic length ($l=8.0$ mm).

Figures 9 and 10 present the modified flow factors (Φ_M) for both seals versus pressure ratio. For the labyrinth seal the data at various temperatures collapses into a single curve, with $\Phi_M \sim 0.25$ at pressure ratios $(P_s/P_a) > 2$ and well into the choked flow conditions. Note the HALO™ seal has a low flow factor (Φ_M) that drops from ~ 0.15 at low pressure ratios to ~ 0.05 at the highest pressure, $(P_s/P_a) \sim 8$, exceptionally high for a clearance seal with short length. The performance of the novel seal improves with pressurization since the operating clearance between rotor and seal pads closes due to the compliance of the structural web supports.

For the HALO™ seal, the flow factor should decrease with increasing shaft speed due to the centrifugal growth of the disc which would reduce the clearance between the test seal and disc.

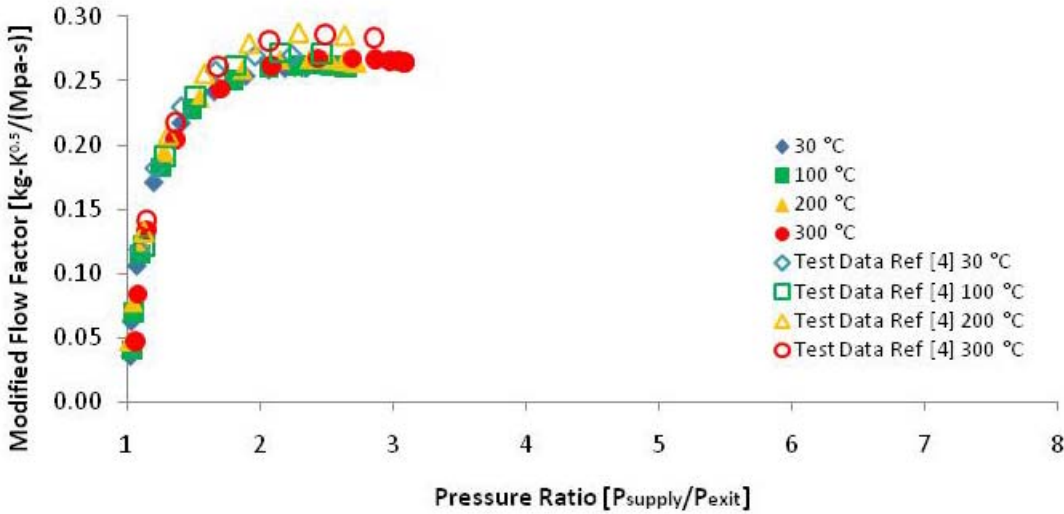


Figure 9. Labyrinth seal: Flow factor Φ_M vs. pressure ratio (P_s/P_a). Tests at increasing air temperatures. Comparison to prior data in Ref. [4]

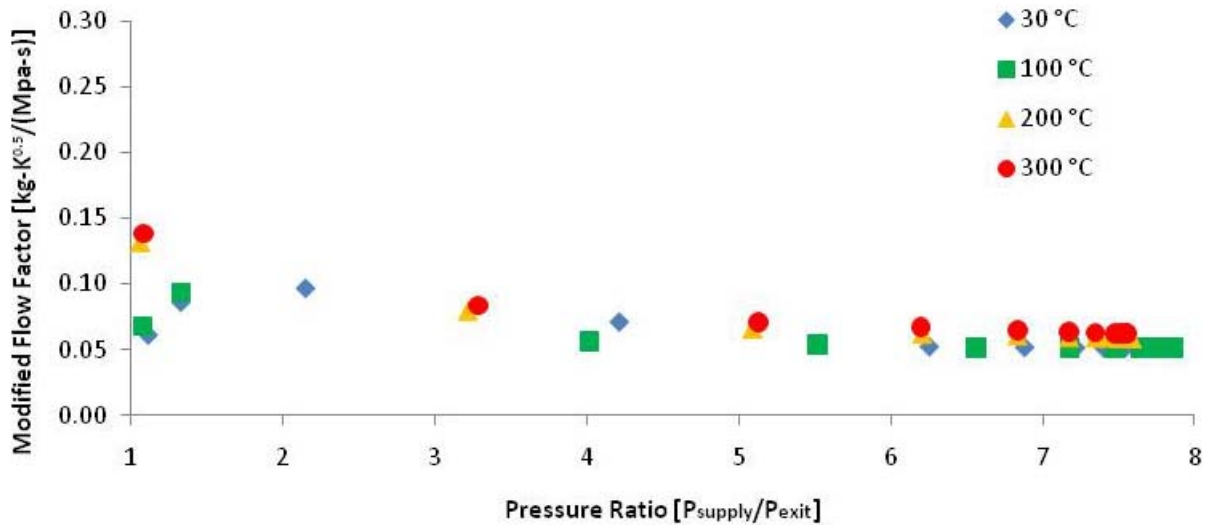


Figure 10. HALO™ seal: Flow factor Φ_M vs. pressure ratio (P_s/P_a). Tests at increasing air temperatures

REVAMPING OF TEST RIG FOR MEASUREMENTS AT HIGH ROTOR SPEEDS

The funded work intends to redesign the rotor assembly system to achieve a top speed of 15 krpm which will render a surface tip speed of 130 m/s with a disc OD~167 mm. The main objective is to measure gas seal leakage and reliability at surface speeds representative of actual turbomachinery, e.g., land-based power generation gas and steam turbines, for example.

Note that the original test rig, see Figures 1 and 2, comprises of a long thin shaft and a massive end disc. A pair of rolling element bearings supports the rotor in cantilevered form. The rotor-bearing system has a very low bending mode natural frequency (~ 20 Hz) with little damping. A test seal, installed on the rotor free end and facing the disc OD, contributes some stiffness and damping to ameliorate rotor vibrations when crossing quickly through a critical speed. Prior tests reported in Ref. [4] were conducted with a rotor speed not exceeding 3,200 rpm (tip speed 27 m/s). The low power of the drive motor and the inherent flexibility of the slender rotor prevented experiments at high speeds. The current configuration is not deemed safe for spinning at motor speeds above 4 krpm.

While keeping in place most existing components in the stationary part of the test rig, namely the pressure vessel and ball bearings' support, the PI outlined several rotor-bearing design concepts to the students whom proceeded to imagine a revamped test rig configuration that in the end, after endless hours of work, could not satisfy the minimum safety and operation requirements, besides exceeding the estimated cost for revamping (\$6.25 k).

In lieu of the cost and time requirements, the PI proposes to keep the original shaft-disc rotor configuration and rolling element support while adding a metal mesh foil bearing (MMFB) support on the free end of the rotor. Figure 11 depicts the original rotor-bearing system with the addition of an air lubricated MMFB. Prior experiences with MMFBs (60 krpm), Refs. [6-9] show their adequacy to operate in high temperature environments by providing both structural stiffness and lots of damping from mechanical hysteresis in the metal mesh.

Figure 12 depicts the MMFB for installation in the test rig and Table 6 details the bearing basic geometry and material properties. Dynamic load measurements (10-300 Hz) conducted with this bearing show it has a structural stiffness (K_B) ~ 0.5 MN/m (2870 lb_f/in) and a material loss factor $\gamma \sim 0.5$. The loss factor is a measure of the ability of the bearing to dissipate mechanical energy. For rotordynamic analysis, the equivalent viscous damping coefficient is $C \sim \gamma K_B / \omega$, with ω as a whirl frequency.

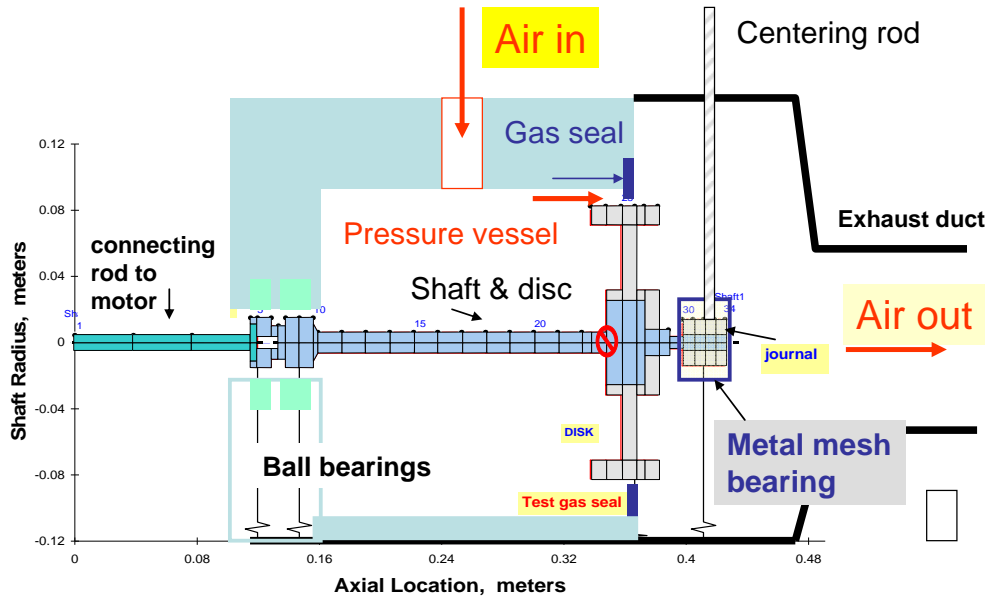


Figure 11. Rotor model with metal mesh foil bearing at free end of rotor

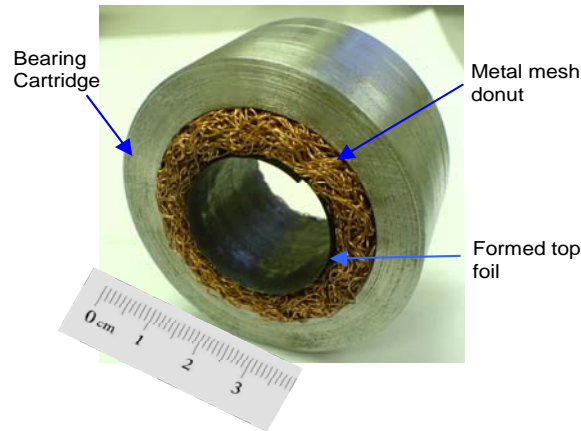


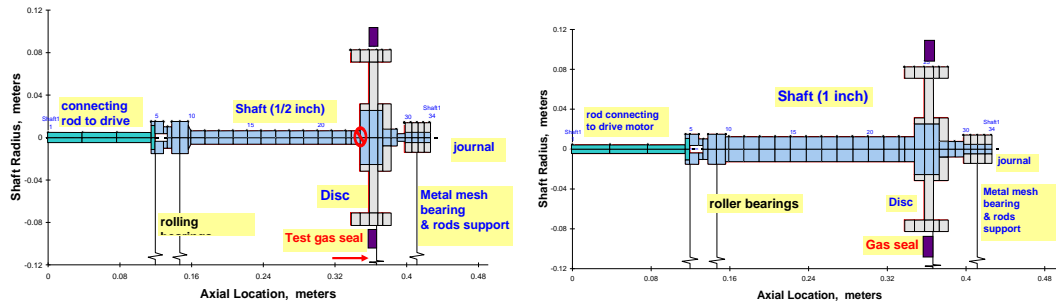
Figure 12. Photograph of Metal Mesh Foil Bearing [6]

Table 6. Dimensions and material specifications for MMFB [6]

Bearing cartridge outer & inner diameters, D_{Bo} & D_{Bi}	58.15 mm, 42.10 ± 0.02 mm
Bearing axial length, L	28.05 mm
Metal mesh outer & inner diameters, D_{MMo} & D_{MMi}	42.10 mm, 28.30 mm
Metal mesh mass, M_m	0.0391 kg
Metal mesh density, ρ_{MM}^2	20 %
Top foil thickness, T_{ff}	0.127 mm
Copper Wire diameter, D_W	0.30 mm
Copper Young modulus, E , at 21 °C	114 GPa
Copper Poisson ratio, ν	0.33
Bearing mass (cartridge + mesh + foil), M	0.318 kg

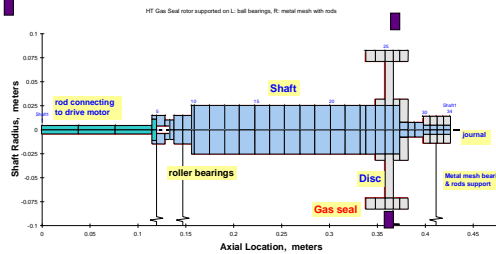
² Manufacturers define the density of metal mesh as the ratio of the ring mass to its volume times the metal material density.

The PI conducted a rotordynamic analysis to find the critical speeds and damping ratios of the modified rotor-bearing system with the MMFB in place. The analysis also considered enlarging the slender shaft OD, from its original 0.5 inch to 2.0 inch. Figure 13 depicts schematic views of the various rotor models. Increasing the shaft OD makes the shaft more rigid and heavier which will raise the rotor first bending mode natural frequency.



(a) original shaft, 1/2 inch OD,

(b) modified shaft to 1 inch OD



(c) modified shaft 2 inch OD

Figure 13. Various rotor models (shaft OD increases) considered for analysis

Table 7 lists the predicted critical speeds and damping ratios for the various rotor configurations analyzed. Note the raise in the first critical speed as the shaft OD increases. The first critical speed increases due to the increase in stiffness of the rotor as it becomes thicker. The damping ratio decreases because the viscous damping coefficient from the MMFB also decreases as the operating frequency increases [7]. The natural mode shapes changes from an elastic cantilever bending mode to a conical more. With the MMFB in place, the system damping ratio (ξ) is quite adequate, ranging from 0.20 to 0.09, as the shaft OD increases.

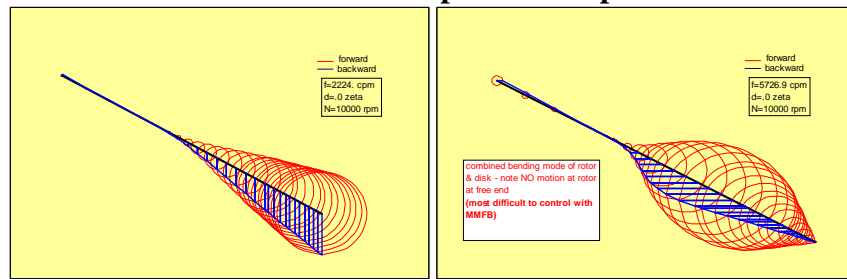
Table 7. Predicted critical speed and damping ratio for rotor supported on MMFB. Shaft diameter varies. Predicted rotor mode shapes at 10 krpm

Shaft diameter inch	Rotor mass kg	Critical speed RPM	Damping ratio	
0.5	4.122	1,500	0.0	w/o MMFB (original)
0.5	4.251	4,511	0.200	with MMFB
1.0	4.821	6,018	0.121	
1.5	5.770	6,550	0.095	
2.0	6.480	6,450	0.090	

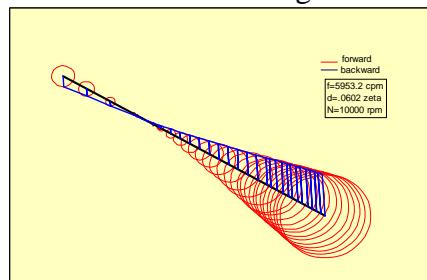
At 15 krpm

Shaft diameter inch	1 st nat frequency RPM	Damping ratio
0.5	4,654	0.046
1.0	6,480	0.046
1.5	6,900	0.039
2.0	6,771	0.036

Rotor mode shapes at 10 krpm



(a) Shaft 0.5 inch OD – original configuration



(b) Shaft 0.5 inch OD – with MMFB support

Figure 14 depicts the rotor amplitude synchronous response at the disc location versus shaft speed. The imbalance is $u=0.01$ gm-cm at the disc (1.2 gram at the disc OD). Note that a thicker shaft will produce larger amplitude of response at the critical speed. Responses at the design

speed of 15 krpm are similar in amplitude for all rotors. In lieu of the predictions below, the original slender shaft (0.5 in OD) will be kept in the revamped test rig.

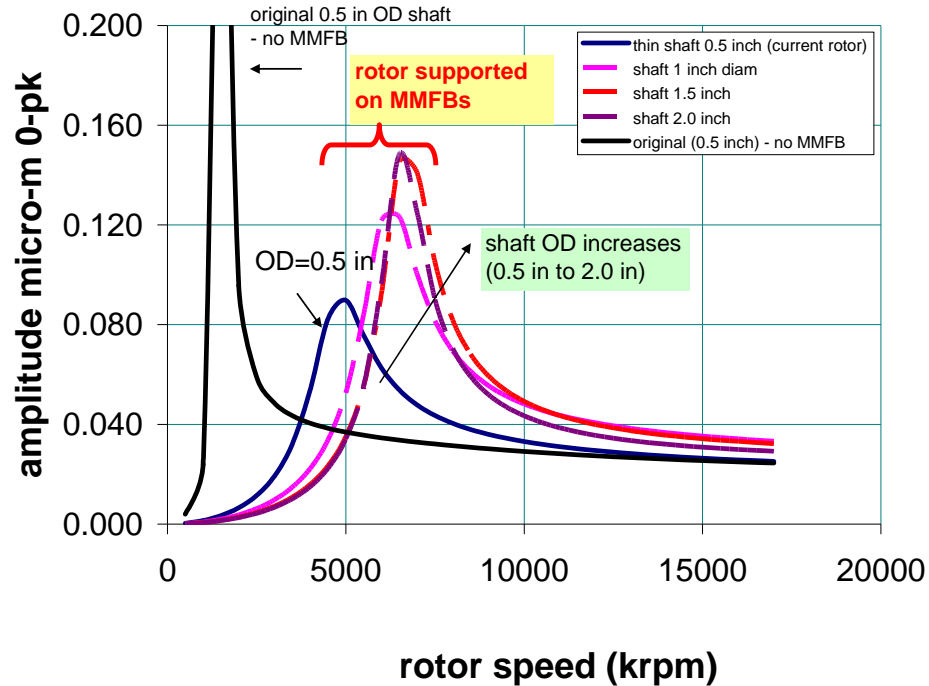


Figure 14. Amplitude of rotor synchronous response at disc location for various shaft OD configurations. Imbalance $u=0.01$ gm-cm at disc outboard

CLOSURE

Labyrinth seals are clearly an outdated technology. At present, there are other seal types that can perform better in terms of leakage reduction and low drag power losses. Industries seeking to increase efficiency by reducing (parasitic) secondary leakage losses will benefit greatly from a change in seal technology [2].

Pressurized air tests with both a labyrinth seal and a novel all metal seal, the HALO™ seal, at high temperature (max 300 C) show the HALO™ seal gives a significant decrease in leakage and the ability to operate in high pressure environments where a labyrinth seal could not.

The graduate student supported by the project will continue planned work (see Table 2) to complete revamping the test rig for high speed operation reaching a tip speed of ~120 m/s and to perform leakage tests with both seals and at increasing air inlet temperatures.

REFERENCES

- [1] Chupp, R. E., Johnson, R. P., and Loewenthal, R. G., 1995, "Brush Seal Development for Large Industrial Gas Turbines," AIAA Paper No. 1995-3146.
- [2] San Andrés, L., and Ashton, Z., 2009, "Monthly Report No. 16: May," Technical Report to Siemens Power Gen., TEES Project 32525/34650/ME.
- [3] San Andrés, L., and Ashton, Z., 2010, "Comparison of Leakage Performance in Three Types of Gas Annular Seals Operating at a High Temperature (300°C)," *Tribol. Trans.*, **53**(3), pp. 463-471.
- [4] Ashton, Z., 2009, "High Temperature Leakage Performance of a Hybrid Brush Seal Compared to a Standard Brush Seal and a Labyrinth Seal," M.S. thesis, Texas A&M University, College Station, TX.
- [5] Delgado, I. R., and Proctor, M. P., 2006, "Continued Investigation of Leakage and Power Loss Test Results for Competing Turbine Engine Seals," AIAA Paper No. 2006-4754.
- [6] San Andrés, L., Chirathadam, T. A., Kim, T., 2010, "Measurement of Structural Stiffness and Damping Coefficients in a Metal Mesh Foil Bearing," *ASME J. Eng. Gas Turbines Power*, **132**(3), p. 032503.
- [7] San Andrés, L., and Chirathadam T.A., 2011, "Identification of Rotordynamic Force Coefficients of a Metal Mesh Foil Bearing Using Impact Load Excitations," *ASME J. Eng. Gas Turbines Power*, vol. 133 (Nov), 112501 [[ASME paper GT2010-22440](#)]
- [8] San Andrés, L., Chirathadam, T., Ryu, K., and Kim, T.H., 2010, "Measurements of Drag Torque, Lift-Off Journal Speed and Temperature in a Metal Mesh Foil Bearing," *ASME J. Eng. Gas Turbines Power*, **132**(11), p. 112503 (1-7)
- [9] San Andrés, L., and Chirathadam, T., 2011, "Metal Mesh Foil Bearings: Effect of Excitation Frequency on Rotordynamic Force Coefficients," [ASME Paper GT2011-45257](#).

Appendix A. BRIEF REVIEW OF LITERATURE ON NON-CONTACTING GAS SEALS: LABYRINTH, BRUSH AND AN ALL METAL SEAL

By Alain Anderson, R.A., edited profusely by Dr. Luis San Andrés

Turbomachinery seals are designed to maintain efficiency by minimizing leakage; therefore, seal design is the most cost-effective measure to increase performance by restricting secondary leakage. Operation at higher gas temperature and pressure and rotor speed aims to increase efficiency, and hence seals must be able to limit flow while enduring severe operating conditions [1].

The review details the purpose, usage, and requirements of three types of seals often used in steam and gas turbines; namely, labyrinth seals, brush seals and their variants such as the hybrid brush seals, and a more modern seal type, an all-metal compliant seal (HALO™) with improved leakage characteristics.

Refer to Chupp et al. [2] for a comprehensive review of the purpose and importance of sealing in turbomachinery, specifically in gas and steam turbines. In these applications mechanical elements sealing secondary flows, i.e., seals to reduce leakage, operate at temperatures up to 600 °C, differential pressures up to 21 bar, and withstand surface speeds up to 400 m/s [2]. These extreme operating conditions, demanding of seals with specialized materials and configurations, create particular challenges to establish reliable seal performance and seal life.

Labyrinth Seals in gas and steam turbines are an effective and inexpensive method of reducing parasitic secondary flows. Labyrinth seals (LS) are clearance (non contact) seals that permit controlled leakage by dissipating flow energy through a series of cavities as seen in Fig. A.1. Once the gas crosses a series of cavities it emerges at the other end of the labyrinth seal at a significantly reduced pressure [3]. Simple in design makes labyrinth seals adaptable to a wide range of sizes and operating conditions. LSs have several disadvantages including high leakage levels which can result in damage to components with due to particle ingestion and wear due to intermittent contact with its rotor [4]; and importantly enough, the potential to generate cross coupled stiffness and negative damping that could induce rotordynamic instabilities. Recent improvements, however, have made LSs more efficient and less prone to dynamic instability [5].

The clearance between the rotor and the tips of the seal teeth determine the sealing leakage efficiency. In practice, the operating clearance increases because of intermittent contact and wear during machine start up and shutdown. In high temperature environments, labyrinth seal designs must also allow for thermal expansion of the seal and rotor.

Childs and Scharrer [6] tested labyrinth seals with teeth on rotor and varying the seal clearance to radius ratios $(c/R)=4.14-7.59 \cdot 10^{-3}$. The authors report that seal cross-coupled stiffness increases with increasing clearances and with increasing shaft speed. Small clearances may cause damage to the rotor and components by contact, especially at high rotor speeds and with large rotor vibration [7].

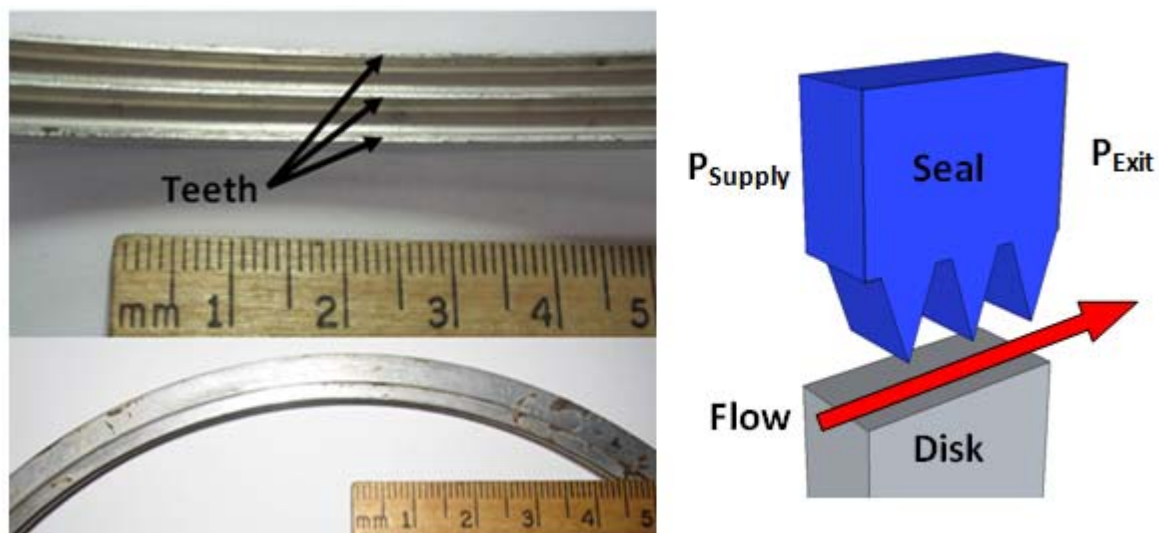


Fig. A.1. Inner side view of a three tooth labyrinth seal and schematic view of thru flow

The necessity for improved performance led to design modifications such as steps, honeycomb lands, and abradable contact surfaces [5]. With these improvements, the seal tooth operate at lower clearance and with better wear characteristics in the case of radial contact. The wear ultimately rubs the seal inner diameter until an adequate clearance develops. However, these designs work on the principle that a high pressure gas flow is delayed by the presence of a sharp-edged obstruction which leads to a lower pressure in the succeeding cavity. To add flow resistance, additional labyrinths can be placed in parallel thus decreasing further leakage.

Finally note that labyrinth seals can be manufactured as rings or segmented to facilitate installation, specifically for large land-based gas turbines. As per Floyd [4], there are no

limitations to the surface speed and pressure differential in which non-contacting seals, such as the labyrinth seal, can endure. El-Gamal et al. [8] state that shaft speed has little effect on the leakage performance of straight through labyrinth seals such as a three tooth labyrinth seal. Shaft rotation does affect some types of labyrinth seals and improves the leakage performance of up-the-step seals and has an adverse effect on down-the-step seal [8].

In aero-gas turbines demanding savings in space and efficiency, brush seals (BS) can replace labyrinth seals. A well designed and installed BS leaks $\sim 1/10$ of the thru flow in a comparably sized labyrinth seal and will not incite rotordynamic instability [9].

Brush Seals consist of a bed of densely packed bristles attached to an outer ring with a backing plate, see Fig A.2. The backing plate prevents the bristles from deforming axially under high pressure differentials. The bristles are designed to contact the rotor during operation which prevents air from entering through the dense bristle pack. Persistent contact with the rotor wears the bristles tips and allows for a clearance to develop, then the BS leakage rate will dramatically increase [10].

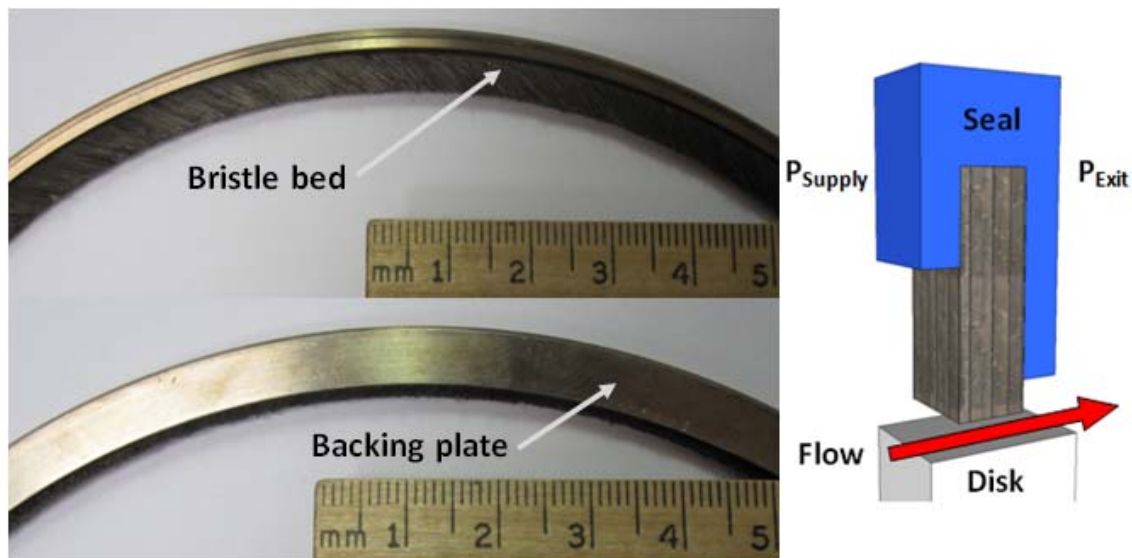


Fig. A.2. Inner side view of a brush seal and schematic view of thru flow

Note that because of the high resilience of the BS bristles, BSs can withstand large rotor radial excursions without damage. The pressure difference across the seal also induces bristles' blow-down, i.e., a pull-like displacement towards the rotor that closes the clearance or gap and further minimizes leakage. However, the brush seal reduces leakage best when in contact with its

rotor [9]. Alas persistent contact increases drag torque and induces localized heat generation and severe thermal distortion is not infrequent.

Generally, BS are designed to rub until an adequate level of interference is achieved, i.e., a break-in period; therefore, some design allowances exist to minimize leakage while averting thermal instability of a brush seal due to excessive contact. High temperature operation degrades mechanical properties and bristle tips wear out sooner than under ambient condition operation.

Note that a BS can be installed in one direction only, with the bristles in the direction of rotor spinning. Reverse rotor rotation or improper BS installation will most likely destroy or permanently deform the seal [2]. BSs also have poor axial stiffness since the bristles tend to bend in the direction of the pressure differential. Since the axial bend is dictated by the length the bristles extending beyond the backing support plate, if the bristles are too long and the bending is excessive, the bristle tips may disengage from the rotor and permit a large amount of leakage [10].

Hybrid Brush Seals (HBS) have evolved to reduce the known disadvantages of BSs, even allowing for bi-directional shaft rotation, albeit increasing the element mechanical complexity.

Hybrid Brush Seals (HBS), as seen in Fig. A.3, incorporate cantilevered (flexural supports) pads at the end of the bristle matrix in a conventional BS. During operation, the cantilever pads generate a hydrodynamic film that lifts the pads whose support elastic elements and bristles have low radial stiffness [11]. Because the pads undergo hydrodynamic lift during operation, the HBS has little heat generation and drag power losses. The gas film prevents any contact between the seal and rotor while permitting a low amount of leakage through.

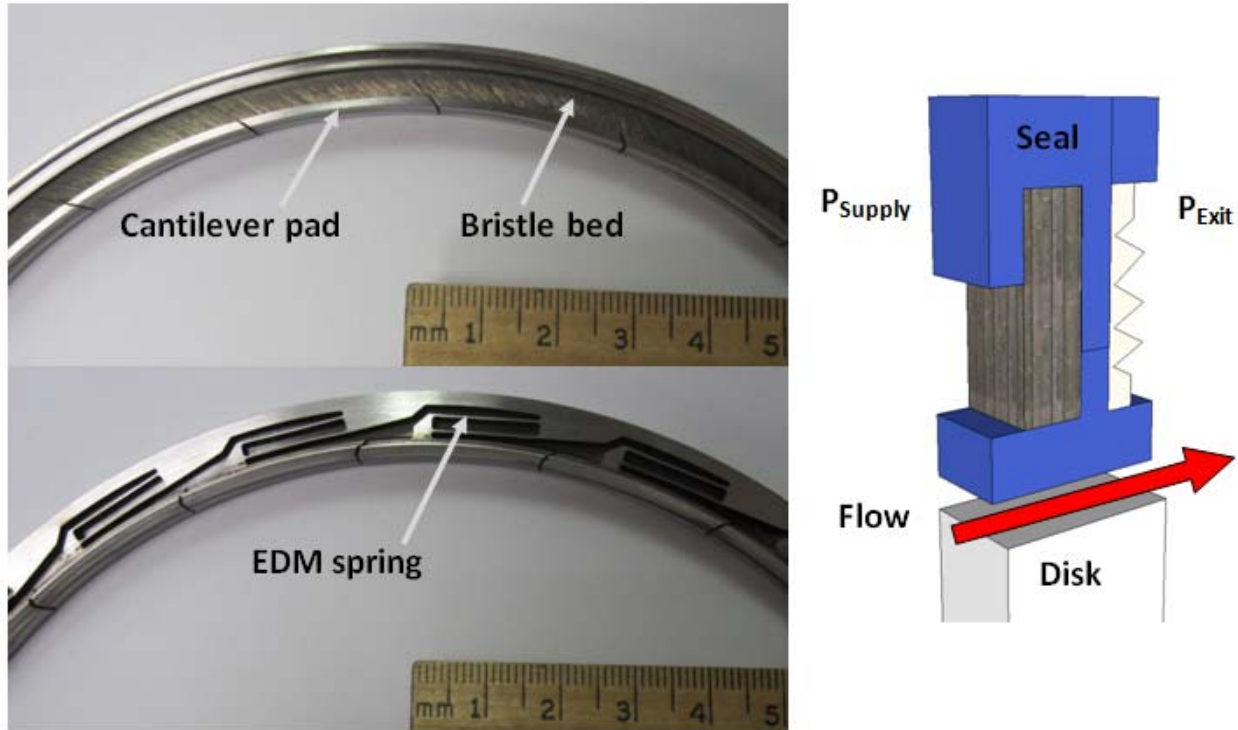


Fig. A.3. Inner side view of a hybrid brush seal and schematic view of thru flow

One HBS demonstrates reduced gas leakage by 36% than a 1st generation shod brush seal [12]. The HBS design calls for a larger axial stiffness which enables the seal to operate at higher pressure differentials [12]. Note however, the HBS has a larger drag torque under unpressurized conditions such as those during machine start-up and shut-down, since the air film is lost and contact ensues with the rotor. The HBS can be slightly off center during assembly since each cantilever pad will lift-off once rotation begins [7].

The Hydrostatic Advanced Low-Leakage (HALO™) Seal is a seal type evolving from the HBS. This novel seal is an all metal compliant seal designed with self-controlling clearance as the pressure differential increases [13]. Of significant note, the HALO™ seal excludes the bristle matrix that is characteristic of a brush seal thus providing a considerably higher axial stiffness. The HALO™ seal consists of cantilevered pads positioned at the inlet of the flow, not at the exit as with prior versions of the HBS. A downstream back wall averts the flow from exceeding beyond the cantilevered pad and, instead, the gas flows in the gap between the rotor and the pads' inner surface.

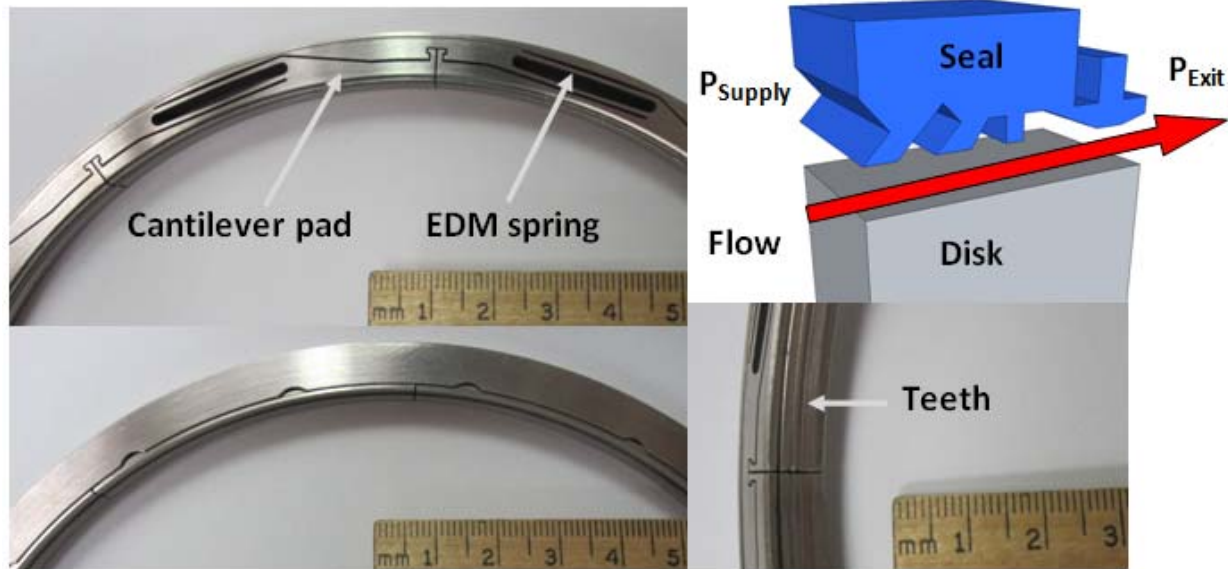


Fig. A.4. Inner side view of a HALO™ seal and schematic view of thru flow

The HALO™ seal is made of steel and assemble with an initial clearance with the rotor. The HBS has its pads with a small converging taper along the axial direction whereas the pads in the HALO™ seal have three slanted grooves at various angles before leading to a convergence as seen in Fig.A.4. Furthermore, the HALO™ seal has a leading (upstream) edge lip intended to draw the pad closer to the disc surface when the seal experiences a pressure differential.

In proprietary tests conducted by San Andrés and Ashton [13], the HALO™ seal reveals the lowest flow factor, an estimated 1/3 that of a similar size HBS and an order of magnitude lower than that for a three tooth labyrinth seal. The data confirms the HALO™ seal excellent sealing features and the potential it has to revolutionize sealing technology in gas and steam turbines.

To continue the progress of this innovative seal technology, the HALO™ seal leakage, drag torque and wear rate must be quantified for operating temperatures, pressure differentials, and rotor speeds representative of gas and steam turbines. These comparisons will evidence the suitability of the HALO™ seal to reduce leakage (secondary flows) in high performance turbomachinery.

References for Appendix A

- [1] Delgado, I. R., and Proctor, M. P., 2006, "Continued Investigation of Leakage and Power Loss Test Results for Competing Turbine Engine Seals," AIAA Paper No. 2006-4754.

- [2] Chupp, R. E., Hendricks, R. C., Lattime, S. B., and Steinetz, B. M., 2006, "Sealing in Turbomachinery," *AIAA Journal of Propulsion and Power*, 22(2), pp. 313-349.
- [3] Eser, D., and Kazakia, J. Y., 1995, "Air Flow in Cavities of Labyrinth Seals," *International Journal of Engineering Science*, 33(15), pp. 2309-2326.
- [4] Floyd, C. G., 1986, "Gas Seals for Rotating Shafts," *Tribology International*, 19(4), pp. 204-211.
- [5] Chupp, R. E., Johnson, R. P., and Loewenthal, R. G., 1995, "Brush Seal Development for Large Industrial Gas Turbines," *AIAA Paper No. 1995-3146*.
- [6] Childs, D. W., 1993, *Turbomachinery Rotordynamics: Phenomena, Modeling and Analysis*, John Wiley & Sons, New York.
- [7] Justak, J. F., and Crudgington, P. F., 2006, "Evaluation of a Film Riding Hybrid Seal," *AIAA Paper No. 2006-4932*.
- [8] El-Gamal, H. A., Awad, T. H., and Saber, E. , 1996, "Leakage from Labyrinth Seals Under Stationary and Rotating Conditions," *Tribology International*, 29(4), pp. 291-297.
- [9] Ferguson, J. G., 1988, "Brushes as High Performance Gas Turbine Seals," *ASME Paper No. 88-GT-182*.
- [10] Hendricks, R. C., Carlile, J. A., Liang, A. D., 1993, "Brush Seal Low Surface Speed Hard-Rub Characteristics," *Joint Propulsion Conference and Exhibit, 29th, Monterey, CA*.
- [11] Delgado, A., San Andrés, L., Justak, J. F., 2005, "Measurements of Leakage, Structural Stiffness and Energy Dissipation Parameters in a Shoed Brush Seal," *Sealing Technology*, 2005(12), pp. 7-10.
- [12] San Andrés, L., Baker, J., and Delgado, A., 2009, "Measurements of Leakage and Power Loss in a Hybrid Brush Seal," *Journal of Engineering for Gas Turbines and Power*, 131(1), p. 012505.
- [13] San Andrés, L., and Ashton, Z., 2009, "Monthly Report No. 16: May," *Technical Report to Siemens,* TEES project TEES Project 32525/34650/ME.

Appendix B. CALIBRATION CHARTS FOR INSTRUMENTATION

Pressure Sensors

Three pressure sensors are installed in the test rig to record the pressure upstream of the flow meter, the supply pressure (P_S) in the pressurized vessel and the exit pressure (P_e) in the exhaust pipe. A high temperature pressure sensor is located in the hot air inlet pipe leading to the pressurization chamber to gather P_S . The sensors were calibrated using a dead weight tester to maximum static pressures of 100 psig (~7 bar).

Figure B.1 shows the calibration data, voltage versus pressure for the high temperature pressure sensor (max. operating temperature of 300 °C). The sensor is linear (perfect line curve fit) with a sensitivity of 4.1 mV/psig. The bias or linearity, uncertainty is +/- 0.25% full-scale output (FSO) and the precision or repeatability uncertainty is +/- 0.1% FSO.

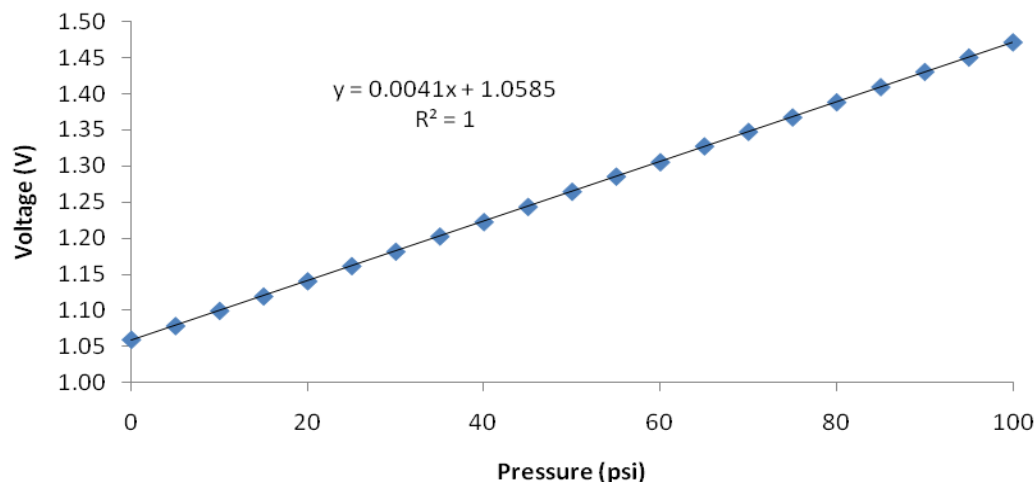


Figure B.1. Voltage (V) versus static pressure for pressure sensor to record supply pressure in high temperature gas seal test rig

Two miniature (Entran and Kulite) pressure sensors collect pressures at the flow meter location and the exhaust chamber. Figure B.2 displays the calibration voltage¹ versus pressure data collected for both sensors to a maximum static pressure of 80 psig. The sensors linearity is 99% or higher and their sensitivity is 1.44 mV/psig and 0.9399 mV/psig. The Kulite sensor has a combined non-linearity and hysteresis uncertainty of +/-0.1 FSO and a precision uncertainty of

¹ The sensors require of a power supply at a well-known voltage. The pressure sensor at the flow meter location requires a DC power supply of 10.77 Volts and the pressure sensor at the exhaust side requires a DC power supply of 10.43 Volts. Changes in the supplied voltage will cause the sensor gain to change.

+/-0.5% FSO. The Entran sensor has a combined non-linearity and hysteresis uncertainty of +/- 0.1 FSO and a precision uncertainty of +/-1.5% FSO.

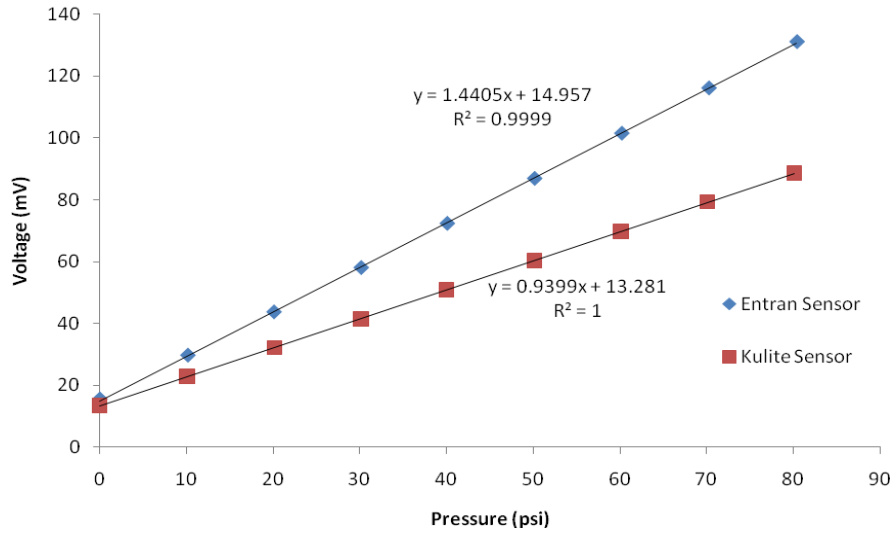


Figure B.2. Voltage (mV) versus static pressure for pressure sensors to record pressure in flow meter and exhaust chamber

Turbine Flowmeter

Figure B.3 shows the manufacturer calibration data for the turbine flow meter (Flow Technology Inc., SN 120872, and Model number FT-12NEYABGEH-5). The flow rate measurements must be conducted at ambient temperature and with at an upstream pressure of 100 psig just before the meter. The manufacturer sensor uncertainty is +/-0.2 SCFM.

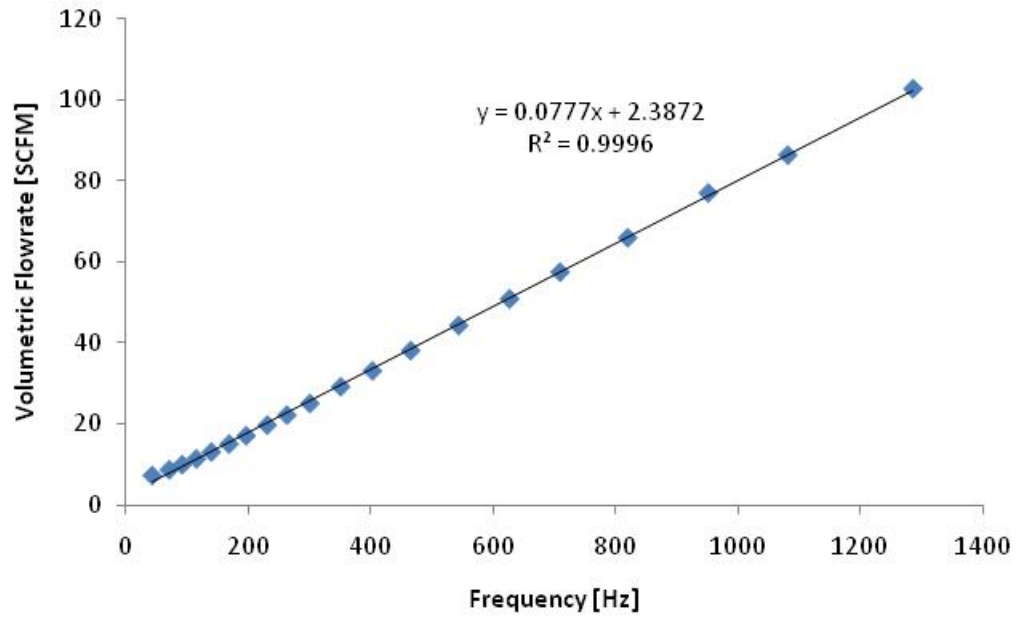


Figure B.3. Volumetric flow rate (SCFM) versus frequency (Hz) in turbine flowmeter